

Revisiting $B_s \rightarrow \mu^+ \mu^-$ and $B \rightarrow K^{(*)} \mu^+ \mu^-$ decays in the MSSM with and without R-parity

Ru-Min Wang^{1,*}, Yuan-Guo Xu¹, Yi-Long Wang¹, Ya-Dong Yang^{2,3}

¹ *College of Physics and Electronic Engineering, Xinyang Normal University, Xinyang, Henan 464000, China*

² *Institute of Particle Physics, Huazhong Normal University, Wuhan, Hubei 430079, P. R. China*

³ *Key Laboratory of Quark & Lepton Physics, Ministry of Education, P.R. China*

November 10, 2018

Abstract

The rare decays $B_s \rightarrow \mu^+ \mu^-$ and $B \rightarrow K^{(*)} \mu^+ \mu^-$ are sensitive to new particles and couplings via their interferences with the standard model contributions. Recently, the upper bound on $\mathcal{B}(B_s \rightarrow \mu^+ \mu^-)$ has been improved significantly by the CMS, LHCb, CDF and DØ experiments. Combining with the measurements of $\mathcal{B}(B \rightarrow K^{(*)} \mu^+ \mu^-)$, we derive constraints on the relevant parameters of minimal supersymmetric standard model with and without R-parity, and examine their contributions to the dimuon forward-backward asymmetry in $B \rightarrow K^* \mu^+ \mu^-$ decay. We find that: (i) the contribution of R-parity violating coupling products $\lambda'_{2i2} \lambda'^*_{2i3}$ due to squark exchange is comparable with the theoretical uncertainties in $B \rightarrow K \mu^+ \mu^-$ decays, but still could be significant in $B \rightarrow K^* \mu^+ \mu^-$ decay and could account for the forward-backward asymmetry in the low dimuon invariant mass region; (ii) three constrained mass insertions $(\delta_{LL}^u)_{23}$, $(\delta_{LL}^d)_{23}$ and $(\delta_{RR}^d)_{23}$ could have significant contribution to $d\mathcal{A}_{FB}(B \rightarrow K^* \mu^+ \mu^-)/ds$, however, only the constrained $(\delta_{LL}^u)_{23}$ effects are favored by the results of the Belle and CDF experiments.

PACS Numbers: 13.20.He, 12.60.Jv, 11.30.Er, 12.15.Mm

*E-mail: ruminwang@gmail.com

1 Introduction

Recently, using $7fb^{-1}$ dataset, the CDF collaboration at Fermilab Tevatron has observed an excess of B_s candidates [1], which is compatible with

$$\mathcal{B}(B_s \rightarrow \mu^+\mu^-) = (1.8_{-0.9}^{+1.1}) \times 10^{-8}, \quad (1)$$

and provided the corresponding upper limit of $\mathcal{B}(B_s \rightarrow \mu^+\mu^-) < 4.0 \times 10^{-8}$ at 95% confidence level (CL).

At the same time, searches for $B_s \rightarrow \mu^+\mu^-$ have also been made by the CMS and LHCb collaborations [2–4], respectively, at the Large Hadron Collider at CERN. The combination of the searches by the CMS and LHCb collaborations results in the upper limits [5]:

$$\mathcal{B}(B_s \rightarrow \mu^+\mu^-) < 1.08 \times 10^{-8} \text{ at 95\% CL}, \quad (2)$$

$$\mathcal{B}(B_s \rightarrow \mu^+\mu^-) < 0.90 \times 10^{-9} \text{ at 90\% CL}, \quad (3)$$

which have improved the previous upper bounds [6] significantly.

$B_s \rightarrow \mu^+\mu^-$ decay is a known sensitive probe to the presence of new physics (NP). In the standard model (SM), it occurs via penguin or box diagrams and is strongly helicity suppressed. Its SM prediction is $(3.2 \pm 0.2) \times 10^{-9}$ [7]. Generally, NP could enhance the $B_s \rightarrow \mu^+\mu^-$ decay rate very much, and thus the upper bound of $\mathcal{B}(B_s \rightarrow \mu^+\mu^-)$ is taken as a strong constraint when a NP model is discussed. As a crossing check, one usually needs to investigate the semileptonic rare decays $B \rightarrow K\mu^+\mu^-$ and $B \rightarrow K^*\mu^+\mu^-$ which are also governed by the flavor changing neutral current (FCNC) transition $b \rightarrow s\mu^+\mu^-$ but not helicity suppressed. Many observables of $B \rightarrow K^{(*)}\mu^+\mu^-$ have been observed by several experiments: BABAR [8], Belle [9] and CDF [10]. As many of them agree with the SM predictions within their error bars, however, the dimuon forward-backward asymmetry of $B \rightarrow K^*\mu^+\mu^-$ present hints of departure from the SM prediction in the low dimuon invariant mass region [11–13].

For NP could alter $\mathcal{B}(B_s \rightarrow \mu^+\mu^-)$, it would consequently alter the observables in $B \rightarrow K^{(*)}\mu^+\mu^-$ decays, for instance, the decay rates as well as the differential branching ratios and the forward-backward asymmetries of $B \rightarrow K^{(*)}\mu^+\mu^-$, from the SM predictions. The NP effects in $b \rightarrow s\mu^+\mu^-$ FCNC transition have been extensively investigated, for instance, in Refs. [14–22]. In this paper, following closely the analysis of Ref. [23], we will update

the constrained R-parity violating (RPV) minimal supersymmetric standard model (MSSM) effects in $B_s \rightarrow \mu^+ \mu^-$ and $B \rightarrow K^{(*)} \mu^+ \mu^-$ decays from the new experimental data. Additionally, we will extend our analysis to the R-parity conserving (RPC) MSSM scenario with the mass insertion (MI) approximation [24, 25]. Using a combination of the limits of $\mathcal{B}(B_s \rightarrow \mu^+ \mu^-)$ from CDF, LHCb and CMS [1, 5] as well as the experimental bounds of $\mathcal{B}(B \rightarrow K^{(*)} \mu^+ \mu^-)$ [26], we will obtain the new limits on the relevant supersymmetric coupling parameters. Then we will use the constrained parameter spaces to examine the their effects on some observables in these decays, especially $d\mathcal{A}_{FB}(B \rightarrow K^* \mu^+ \mu^-)/ds$.

The paper is arranged as follows. In Section 2, we present a very brief theoretical introduction to $B_s \rightarrow \mu^+ \mu^-$ and $B \rightarrow K^{(*)} \mu^+ \mu^-$ processes. In Section 3, we deal with the numerical results. We display the constrained parameter spaces which further satisfy new experimental data, and then we use the constrained parameter spaces to predict the RPV effects and RPC MI effects on the dimuon invariant mass spectra and the dimuon forward-backward asymmetries in $B \rightarrow K^{(*)} \mu^+ \mu^-$ decays, which could differ from the SM expectations. Section 4 contains our conclusion.

2 The theoretical frame for $B_s \rightarrow \mu^+ \mu^-$ and $B \rightarrow K^{(*)} \mu^+ \mu^-$

2.1 The pureleptonic decay $B_s \rightarrow \mu^+ \mu^-$

The branching ratio for $B_s \rightarrow \mu^+ \mu^-$ can be written as [21, 27]

$$\mathcal{B}(B_s \rightarrow \mu^+ \mu^-) = \frac{\tau_{B_s} m_{B_s}^3 f_{B_s}^2}{32\pi} \sqrt{1 - \frac{4m_\mu^2}{m_{B_s}^2}} \left[|F_B|^2 \left(1 - \frac{4m_\mu^2}{m_{B_s}^2} \right) + |F_A|^2 \right], \quad (4)$$

where

$$\begin{aligned} F_A &= \frac{2m_\mu}{m_{B_s}} (C_A - \tilde{C}_A) + m_{B_s} (C_P - \tilde{C}_P), \\ F_B &= m_{B_s} (C_S - \tilde{C}_S). \end{aligned} \quad (5)$$

The SM result for the branching ratio may be obtained from Eq. (4) by setting $\tilde{C}_A = C_S = \tilde{C}_S = C_P = \tilde{C}_P = 0$ and

$$C_A = \frac{G_F \alpha}{\sqrt{2} \pi \sin^2 \theta_W} V_{tb} V_{ts}^* Y(x_t). \quad (6)$$

In the MSSM without R-parity, the branching ratio may be obtained by setting [23]

$$\begin{aligned}
C'_A &= -\frac{\lambda'_{2i2}\lambda'^*_{2i3}}{4m_{\tilde{u}_{iL}}^2}, \\
C_S &= -C_P = -\frac{\lambda_{i22}\lambda'^*_{i23}}{4m_b m_{\tilde{\nu}_{iL}}^2}, \\
C'_S &= C'_P = -\frac{\lambda_{i22}^*\lambda'_{i32}}{4m_b m_{\tilde{\nu}_{iL}}^2}.
\end{aligned} \tag{7}$$

In the MSSM with R-parity, the branching ratio can be obtained by using the expressions C_S, \tilde{C}_S, C_P and \tilde{C}_P can be found in Ref. [21], and $\tilde{C}_A = 0$ in this case.

2.2 The semileptonic decays $B \rightarrow K^{(*)}\mu^+\mu^-$

In the SM, the double differential decay branching ratios $\frac{d^2\mathcal{B}^K}{d\hat{s}d\hat{u}}$ and $\frac{d^2\mathcal{B}^{K^*}}{d\hat{s}d\hat{u}}$ for the decays $B \rightarrow K\mu^+\mu^-$ and $B \rightarrow K^*\mu^+\mu^-$, respectively, may be written as [13]

$$\begin{aligned}
\frac{d^2\mathcal{B}_{SM}^K}{d\hat{s}d\hat{u}} &= \tau_B \frac{G_F^2 \alpha_e^2 m_B^5}{2^{11}\pi^5} |V_{ts}^* V_{tb}|^2 \\
&\times \left\{ (|A'|^2 + |C'|^2)(\lambda - \hat{u}^2) \right. \\
&\left. + |C'|^2 4\hat{m}_\mu^2 (2 + 2\hat{m}_K^2 - \hat{s}) + \text{Re}(C'D'^*) 8\hat{m}_\mu^2 (1 - \hat{m}_K^2) + |D'|^2 4\hat{m}_\mu^2 \hat{s} \right\},
\end{aligned} \tag{8}$$

$$\begin{aligned}
\frac{d^2\mathcal{B}_{SM}^{K^*}}{d\hat{s}d\hat{u}} &= \tau_B \frac{G_F^2 \alpha_e^2 m_B^5}{2^{11}\pi^5} |V_{ts}^* V_{tb}|^2 \\
&\times \left\{ \frac{|A|^2}{4} (\hat{s}(\lambda + \hat{u}^2) + 4\hat{m}_\mu^2 \lambda) + \frac{|E|^2}{4} (\hat{s}(\lambda + \hat{u}^2) - 4\hat{m}_\mu^2 \lambda) \right. \\
&+ \frac{1}{4\hat{m}_{K^*}^2} [|B|^2 (\lambda - \hat{u}^2 + 8\hat{m}_{K^*}^2 (\hat{s} + 2\hat{m}_\mu^2)) + |F|^2 (\lambda - \hat{u}^2 + 8\hat{m}_{K^*}^2 (\hat{s} - 4\hat{m}_\mu^2))] \\
&- 2\hat{s}\hat{u} [\text{Re}(BE^*) + \text{Re}(AF^*)] \\
&+ \frac{\lambda}{4\hat{m}_{K^*}^2} [|C|^2 (\lambda - \hat{u}^2) + |G|^2 (\lambda - \hat{u}^2 + 4\hat{m}_\mu^2 (2 + 2\hat{m}_{K^*}^2 - \hat{s}))] \\
&- \frac{1}{2\hat{m}_{K^*}^2} [\text{Re}(BC^*) (1 - \hat{m}_{K^*}^2 - \hat{s}) (\lambda - \hat{u}^2) \\
&\quad + \text{Re}(FG^*) ((1 - \hat{m}_{K^*}^2 - \hat{s}) (\lambda - \hat{u}^2) + 4\hat{m}_\mu^2 \lambda)] \\
&\left. - 2\frac{\hat{m}_\mu^2}{\hat{m}_{K^*}^2} \lambda [\text{Re}(FH^*) - \text{Re}(GH^*) (1 - \hat{m}_{K^*}^2)] + |H|^2 \frac{\hat{m}_\mu^2}{\hat{m}_{K^*}^2} \hat{s} \lambda \right\},
\end{aligned} \tag{9}$$

where $p = p_B + p_{K^{(*)}}$, $s = q^2$ and $q = p_+ + p_-$ (p_\pm the four-momenta of the leptons), and the auxiliary functions $A - H$ can be found in Ref. [13]. The hat denotes normalization in terms of the B-meson mass, m_B , e.g. $\hat{s} = s/m_B^2$, $\hat{m}_q = m_q/m_B$.

In the MSSM without R-parity, the squark exchange contributions could get from Eqs. (8-9) by the replacements [23]

$$\begin{aligned}
A'(\hat{s}) &\rightarrow A'(\hat{s}) + \frac{f_+^{B \rightarrow K}(\hat{s})}{W} \sum_i \frac{\lambda'_{2i2} \lambda'^*_{2i3}}{8m_{\tilde{u}_{iL}}^2}, \\
C'(\hat{s}) &\rightarrow C'(\hat{s}) - \frac{f_+^{B \rightarrow K}(\hat{s})}{W} \sum_i \frac{\lambda'_{2i2} \lambda'^*_{2i3}}{8m_{\tilde{u}_{iL}}^2}, \\
A(\hat{s}) &\rightarrow A(\hat{s}) + \frac{1}{W} \left[\frac{2V^{B \rightarrow K^*}(\hat{s})}{m_B + m_{K^*}} m_B^2 \right] \sum_i \frac{\lambda'_{2i2} \lambda'^*_{2i3}}{8m_{\tilde{u}_{iL}}^2}, \\
B(\hat{s}) &\rightarrow B(\hat{s}) + \frac{1}{W} \left[-(m_B + m_{K^*}) A_1^{B \rightarrow K^*}(\hat{s}) \right] \sum_i \frac{\lambda'_{2i2} \lambda'^*_{2i3}}{8m_{\tilde{u}_{iL}}^2}, \\
C(\hat{s}) &\rightarrow C(\hat{s}) + \frac{1}{W} \left[\frac{A_2^{B \rightarrow K^*}(\hat{s})}{m_B + m_{K^*}} m_B^2 \right] \sum_i \frac{\lambda'_{2i2} \lambda'^*_{2i3}}{8m_{\tilde{u}_{iL}}^2}, \\
D(\hat{s}) &\rightarrow D(\hat{s}) + \frac{1}{W} \left[\frac{2m_{K^*}}{\hat{s}} (A_3^{B \rightarrow K^*}(\hat{s}) - A_0^{B \rightarrow K^*}(\hat{s})) \right] \sum_i \frac{\lambda'_{2i2} \lambda'^*_{2i3}}{8m_{\tilde{u}_{iL}}^2}, \\
E(\hat{s}) &\rightarrow E(\hat{s}) - \frac{1}{W} \left[\frac{2V^{B \rightarrow K^*}(\hat{s})}{m_B + m_{K^*}} m_B^2 \right] \sum_i \frac{\lambda'_{2i2} \lambda'^*_{2i3}}{8m_{\tilde{u}_{iL}}^2}, \\
F(\hat{s}) &\rightarrow F(\hat{s}) - \frac{1}{W} \left[-(m_B + m_{K^*}) A_1^{B \rightarrow K^*}(\hat{s}) \right] \sum_i \frac{\lambda'_{2i2} \lambda'^*_{2i3}}{8m_{\tilde{u}_{iL}}^2}, \\
G(\hat{s}) &\rightarrow G(\hat{s}) - \frac{1}{W} \left[\frac{A_2^{B \rightarrow K^*}(\hat{s})}{m_B + m_{K^*}} m_B^2 \right] \sum_i \frac{\lambda'_{2i2} \lambda'^*_{2i3}}{8m_{\tilde{u}_{iL}}^2}, \\
H(\hat{s}) &\rightarrow H(\hat{s}) - \frac{1}{W} \left[\frac{2m_{K^*}}{\hat{s}} (A_3^{B \rightarrow K^*}(\hat{s}) - A_0^{B \rightarrow K^*}(\hat{s})) \right] \sum_i \frac{\lambda'_{2i2} \lambda'^*_{2i3}}{8m_{\tilde{u}_{iL}}^2}, \tag{10}
\end{aligned}$$

where $W = -\frac{G_F \alpha_e}{2\sqrt{2} \pi} V_{ts}^* V_{tb} m_B$.

The sneutrino exchanges contributions are summarized as

$$\begin{aligned}
\frac{d^2 \mathcal{B}_{\tilde{\nu}}^K}{d\hat{s} d\hat{u}} &= \tau_B \frac{m_B^3}{2^7 \pi^3} \left\{ \text{Re}(W A' \mathcal{T}_S^*) (2\hat{m}_\ell \hat{u}) + \text{Re}(W C' \mathcal{T}_P^*) (1 - \hat{m}_K^2) (-2\hat{m}_\ell) \right. \\
&\quad \left. + \text{Re}(W D' \mathcal{T}_P^*) (-2\hat{m}_\ell \hat{s}) + |\mathcal{T}_S'|^2 (\hat{s} - 2\hat{m}_\ell^2) \right\}, \tag{11}
\end{aligned}$$

$$\begin{aligned}
\frac{d^2 \mathcal{B}_{\tilde{\nu}}^{K^*}}{d\hat{s} d\hat{u}} &= \tau_B \frac{m_B^3}{2^7 \pi^3} \left\{ -\frac{\hat{m}_\ell^2}{\hat{m}_{K^*}^2} \left[\text{Im}(W B \mathcal{T}_S^*) (\lambda^{-\frac{1}{2}} \hat{u} (1 - \hat{m}_{K^*}^2 - \hat{s})) \right. \right. \\
&\quad \left. + \text{Im}(W C \mathcal{T}_S^*) \lambda^{\frac{1}{2}} \hat{u} - \text{Im}(W F \mathcal{T}_P^*) \lambda^{\frac{1}{2}} \right. \\
&\quad \left. \left. + \text{Im}(W G \mathcal{T}_P^*) \lambda^{\frac{1}{2}} (1 - \hat{m}_{K^*}^2) \right] + |\mathcal{T}_S|^2 (\hat{s} - 2\hat{m}_\ell^2) \right\}, \tag{12}
\end{aligned}$$

with

$$\mathcal{T}_S' = f_+^{B \rightarrow K}(\hat{s}) \frac{m_B^2 - m_K^2}{\overline{m}_b - \overline{m}_s} \sum_i \left(\frac{\lambda_{i22}^* \lambda'_{i32}}{8m_{\tilde{\nu}_{iL}}^2} + \frac{\lambda_{i22} \lambda'_{i23}}{8m_{\tilde{\nu}_{iL}}^2} \right),$$

$$\begin{aligned}
\mathcal{T}'_P &= f_+^{B \rightarrow K}(\hat{s}) \frac{m_B^2 - m_K^2}{\overline{m}_b - \overline{m}_s} \sum_i \left(\frac{\lambda_{i22}^* \lambda'_{i32}}{8m_{\tilde{\nu}_{iL}}^2} - \frac{\lambda_{i22} \lambda_{i23}^*}{8m_{\tilde{\nu}_{iL}}^2} \right), \\
\mathcal{T}_S &= \left[\frac{i}{2} \frac{A_0^{B \rightarrow K^*}(\hat{s})}{\overline{m}_b + \overline{m}_s} \lambda^{\frac{1}{2}} m_B^2 \right] \sum_i \left(\frac{\lambda_{i22}^* \lambda'_{i32}}{8m_{\tilde{\nu}_{iL}}^2} - \frac{\lambda_{i22} \lambda_{i23}^*}{8m_{\tilde{\nu}_{iL}}^2} \right), \\
\mathcal{T}_P &= \left[\frac{i}{2} \frac{A_0^{B \rightarrow K^*}(\hat{s})}{\overline{m}_b + \overline{m}_s} \lambda^{\frac{1}{2}} m_B^2 \right] \sum_i \left(\frac{\lambda_{i22}^* \lambda'_{i32}}{8m_{\tilde{\nu}_{iL}}^2} + \frac{\lambda_{i22} \lambda_{i23}^*}{8m_{\tilde{\nu}_{iL}}^2} \right).
\end{aligned} \tag{13}$$

In the MSSM with R-parity, all the effects arise from the RPC MIs contributing to C_7 , \tilde{C}_9^{eff} , \tilde{C}_{10} , and they are

$$\begin{aligned}
C_7^{RPC} &= C_7^{Diag} + C_7^{MI}, \\
(\tilde{C}_9^{eff})^{RPC} &= (\tilde{C}_9^{eff})^{Diag} + (\tilde{C}_9^{eff})^{MI}, \\
\tilde{C}_{10}^{RPC} &= \tilde{C}_{10}^{Diag} + \tilde{C}_{10}^{MI},
\end{aligned} \tag{14}$$

where $C_7^{Diag,MI}$, $(\tilde{C}_9^{eff})^{Diag,MI}$ and $\tilde{C}_{10}^{Diag,MI}$ have been estimated in Refs. [28, 29]. The results for \mathcal{B}^K and \mathcal{B}^{K^*} including MI effects can be obtained from Eqs. (8-9) by following replacements [19, 22]

$$\begin{aligned}
C_7^{SM} &\rightarrow C_7^{SM} + C_7^{RPC}, \\
(C_9^{eff})^{SM} &\rightarrow (C_9^{eff})^{SM} + (\tilde{C}_9^{eff})^{RPC}, \\
C_{10}^{SM} &\rightarrow C_{10}^{SM} + \tilde{C}_{10}^{RPC}
\end{aligned} \tag{15}$$

for decay $B \rightarrow K\mu^+\mu^-$ as well as for the terms related to the form factors V and T_1 in $B \rightarrow K^*\mu^+\mu^-$ decay,

$$\begin{aligned}
C_7^{SM} &\rightarrow C_7^{SM} + C_7^{RPC}, \\
(C_9^{eff})^{SM} &\rightarrow (C_9^{eff})^{SM} - (\tilde{C}_9^{eff})^{RPC}, \\
C_{10}^{SM} &\rightarrow C_{10}^{SM} - \tilde{C}_{10}^{RPC}
\end{aligned} \tag{16}$$

for the terms related to the form factors A_0, A_1, A_2, T_2 and T_3 in $B \rightarrow K^*\mu^+\mu^-$ decay.

From the total double differential branching ratios, we can get the dimuon forward-backward asymmetries [13]

$$\mathcal{A}_{FB}(B \rightarrow K^{(*)}\mu^+\mu^-) = \int d\hat{s} \frac{\int_{-1}^{+1} \frac{d^2\mathcal{B}(B \rightarrow K^{(*)}\mu^+\mu^-)}{d\hat{s}d\cos\theta} \text{sign}(\cos\theta) d\cos\theta}{\int_{-1}^{+1} \frac{d^2\mathcal{B}(B \rightarrow K^{(*)}\mu^+\mu^-)}{d\hat{s}d\cos\theta} d\cos\theta}. \tag{17}$$

3 Numerical results and analysis

We will present our numerical results and analysis in this section. When we study the effects due to MSSM with and without R-parity, we consider only one new coupling product at one time, neglecting the interferences between different new coupling products, but keeping their interferences with the SM amplitude. The input parameters are collected in Appendix, and the following experimental data will be used to constrain parameters of the relevant new couplings [5, 26]

$$\begin{aligned}\mathcal{B}(B_s \rightarrow \mu^+ \mu^-) &< 9 \times 10^{-9} \text{ (at the 90\% CL)}, \\ \mathcal{B}(B \rightarrow K \mu^+ \mu^-) &= (0.48 \pm 0.06) \times 10^{-6}, \\ \mathcal{B}(B \rightarrow K^* \mu^+ \mu^-) &= (1.15 \pm 0.15) \times 10^{-6}.\end{aligned}\tag{18}$$

To be conservative, we use all input parameters and experimental data at the 90% CL in our numerical results. We do not impose the experimental bounds from $d\mathcal{A}_{FB}(B \rightarrow K^* \mu^+ \mu^-)/ds$ and leave it as predictions of the restricted parameter spaces of the two NP scenarios, and compare them with the experimental results.

3.1 RPV MSSM effects

Firstly, we will consider the RPV effects and further constrain the relevant RPV couplings from the new experimental data of $\mathcal{B}(B_s \rightarrow \mu^+ \mu^-)$ and $\mathcal{B}(B \rightarrow K^{(*)} \mu^+ \mu^-)$ given in Eq. (18). As given in Sec. 2, there are three RPV coupling products, which are $\lambda'_{2i2} \lambda_{2i3}^*$ due to squark exchange as well as $\lambda_{i22} \lambda_{i23}'^*$ and $\lambda_{i22}^* \lambda_{i32}'$ due to sneutrino exchange, relevant to $B_s \rightarrow \mu^+ \mu^-$ and $B \rightarrow K^{(*)} \mu^+ \mu^-$ decays.

Our new bounds for three RPV coupling products from the 90% CL experimental data are demonstrated in Fig. 1. And the upper limits for the relevant RPV coupling products by $\mathcal{B}(B \rightarrow K^{(*)} \mu^+ \mu^-)$ and $\mathcal{B}(B_s \rightarrow \mu^+ \mu^-)$ are summarized in Table 1. For comparison, our previous bounds on these quadric coupling products are also listed. From Fig. 1 and Table 1, one can find that all three RPV coupling products are restricted, and the upper limits of $|\lambda_{i22} \lambda_{i32}'^*|$ and $|\lambda_{i22}^* \lambda_{i32}'|$ are improved by about a factor of 2 by the new experimental data. Notice that we assume the masses of sfermions are 500 GeV. For other values of the sfermion

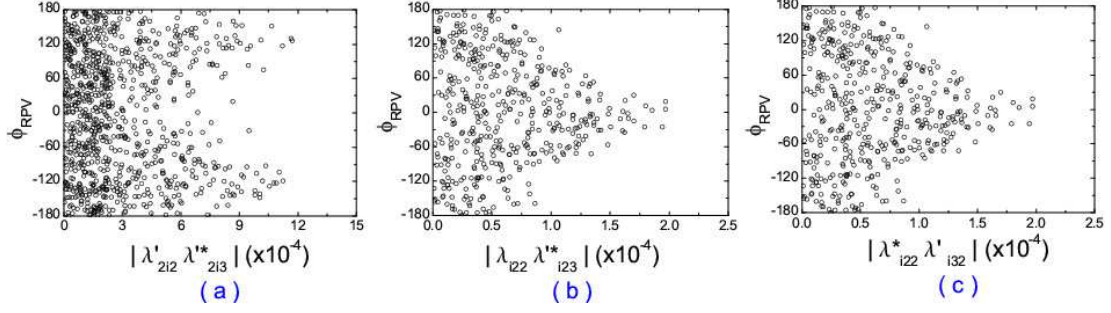


Figure 1: The allowed RPV parameter spaces with 500 GeV sfermions, and the RPV weak phase (ϕ_{RPV}) is given in degree.

Table 1: Bounds for the relevant RPV coupling products by $B \rightarrow K^{(*)}\mu^+\mu^-$ and $B_s \rightarrow \mu^+\mu^-$ decays for 500 GeV sfermions, and previous bounds are listed for comparison.

Couplings	Bounds	Previous bounds [23]
$ \lambda'_{2i2}\lambda_{2i3}^* $	$\leq 11.1 \times 10^{-4}$	$\leq 11.5 \times 10^{-4}$
$ \lambda_{i22}\lambda_{i32}^* $	$\leq 2.0 \times 10^{-4}$	$\leq 4.5 \times 10^{-4}$
$ \lambda_{i22}^*\lambda'_{i23} $	$\leq 2.0 \times 10^{-4}$	$\leq 4.3 \times 10^{-4}$

masses, the bounds on the couplings in this paper can be easily obtained by scaling them by factor of $\tilde{f}^2 \equiv (\frac{m_{\tilde{f}}}{500\text{GeV}})^2$.

Now we will analysis the constrained RPV effects on $\mathcal{B}(B_s \rightarrow \mu^+\mu^-)$. The sensitivities of $\mathcal{B}(B_s \rightarrow \mu^+\mu^-)$ to the constrained RPV couplings are shown in Fig. 2. The limits of the measurements at the 90% CL and the SM predictions with 1.64σ theoretical uncertainties are also displayed in Fig. 2 for convenient comparison. Figs. 2 (a) and (b) show the constrained effects of the modulus and weak phase of t-channel squark exchange coupling $\lambda'_{2i2}\lambda_{2i3}^*$, respectively. As shown in Figs. 2 (a-b), with the contribution of $\lambda'_{2i2}\lambda_{2i3}^*$ included, $\mathcal{B}(B_s \rightarrow \mu^+\mu^-)$ is lower than its experimental upper limit [5]. Besides the constraints from $\mathcal{B}(B_s \rightarrow K^{(*)}\mu^+\mu^-)$, $\lambda'_{2i2}\lambda_{2i3}^*$ coupling is not further constrained by the new experimental upper limit from CMS and LHCb since its contribution to $\mathcal{B}(B_s \rightarrow \mu^+\mu^-)$ is suppressed by m_μ^2/m_B^2 . Additionally, the allowed parameter space of $\lambda'_{2i3}\lambda_{2i2}^*$ would be excluded if the 68% CL experimental determination $\mathcal{B}(B_s \rightarrow \mu^+\mu^-) = (1.8_{-0.9}^{+1.1}) \times 10^{-8}$ [1] by the CDF collaboration were taken as constraint. Two s-channel sneutrino exchange contributions to $\mathcal{B}(B_s \rightarrow \mu^+\mu^-)$ are very similar

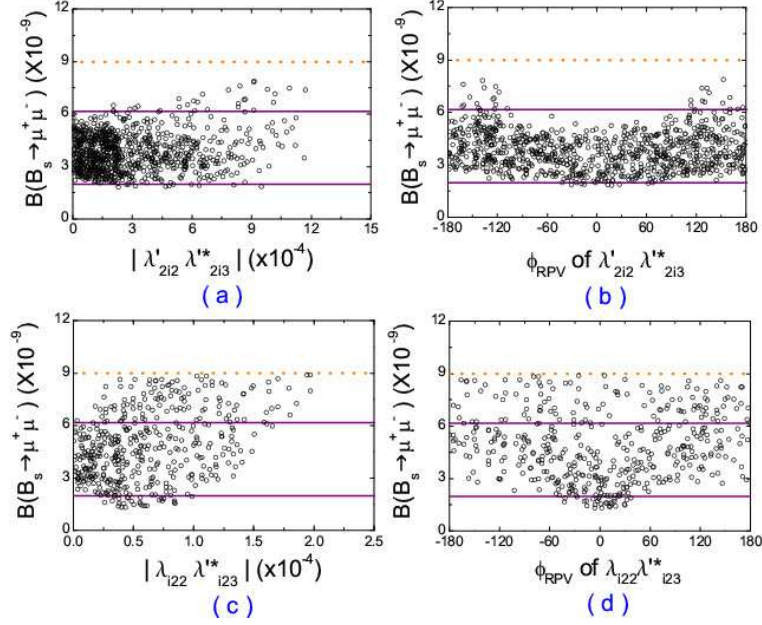


Figure 2: The constrained RPV coupling effects on $\mathcal{B}(B_s \rightarrow \mu^+ \mu^-)$. The orange(violet) horizontal dashed(solid) lines denote the limits of the measurements(SM predictions) at the 90% CL.

to each other. We would take $\lambda_{i22} \lambda'^*_{i23}$ contribution as an example, which is shown by Figs. 2 (c-d). We can see that $\mathcal{B}(B_s \rightarrow \mu^+ \mu^-)$ is sensitive to both the modulus and phase of $\lambda_{i22} \lambda'^*_{i23}$, and $\mathcal{B}(B_s \rightarrow \mu^+ \mu^-)$ could be increased but also could be decreased by the presence of $\lambda_{i22} \lambda'^*_{i23}$ coupling. Generally, the $\lambda_{i22} \lambda'^*_{i23}$ coupling could alter $\mathcal{B}(B_s \rightarrow \mu^+ \mu^-)$ significantly since it's contribution is not helicity suppressed by m_μ^2/m_B^2 . Thus, the constraint on $\lambda_{i22} \lambda'^*_{i23}$ is due to the bound of $\mathcal{B}(B_s \rightarrow \mu^+ \mu^-)$ [5].

Then we turn to analysis the constrained RPV effects in the $B \rightarrow K^{(*)} \mu^+ \mu^-$ decays. Using the new constrained parameter spaces shown in Fig. 1, we will give the RPV effects on the dimuon invariant mass spectra and the forward-backward asymmetries of $B \rightarrow K^{(*)} \mu^+ \mu^-$ decays. In Fig. 3, we present correlations between the dimuon invariant mass spectra as well as the dimuon forward-backward asymmetries and the parameter spaces of $\lambda'_{2i3} \lambda'^*_{2i2}$ by the two-dimensional scatter plots. The dimuon invariant mass distribution and the dimuon forward-backward asymmetry are given with vector meson dominance contribution excluded in terms of $d\mathcal{B}/d\hat{s}$ and $d\mathcal{A}_{FB}/d\hat{s}$, and included in $d\mathcal{B}'/d\hat{s}$ and $d\mathcal{A}'_{FB}/d\hat{s}$, respectively. The theoretical uncertainties of new RPV predictions shown in Fig. 3 are smaller than previous one in Ref. [23].

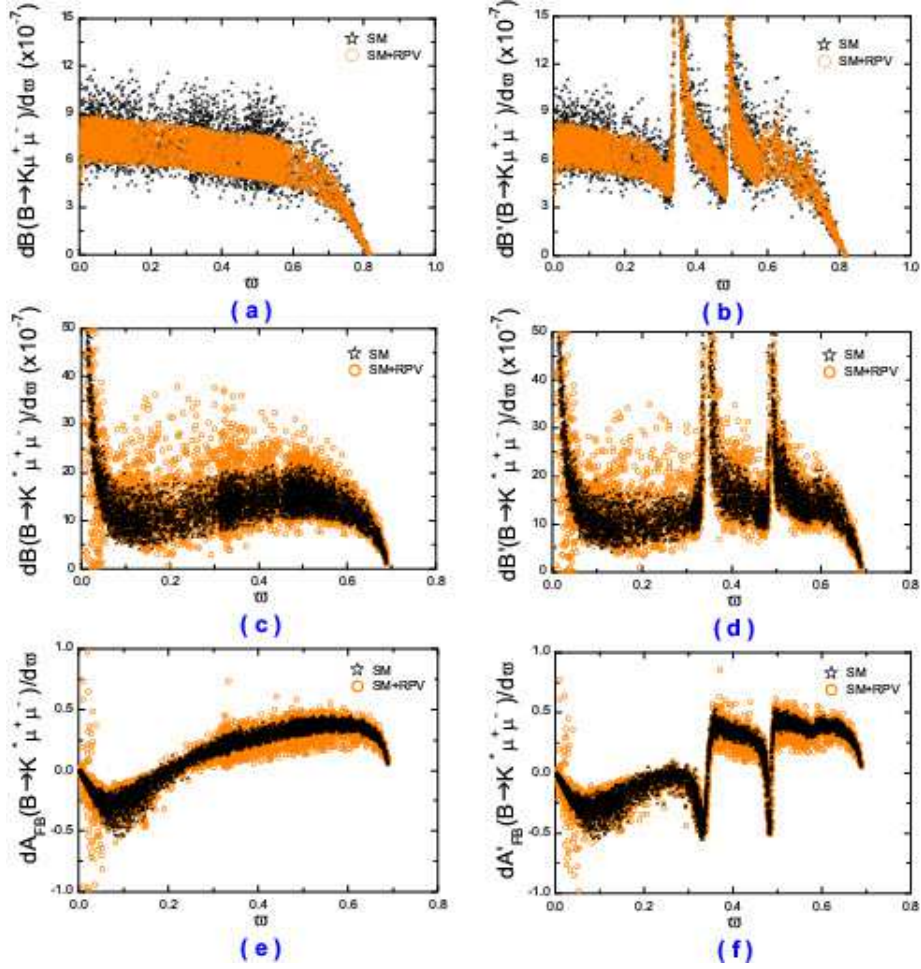


Figure 3: The effects of RPV coupling $\lambda'_{2i2}\lambda_{2i3}^*$ due to the squark exchange in $B \rightarrow K^{(*)}\mu^+\mu^-$ decays, and ϖ denotes \hat{s} .

The RPV effects on $d\mathcal{A}'_{FB}(B \rightarrow K^*\mu^+\mu^-)/d\hat{s}$ are shown in Fig. 3 (f). This observable has been measured as a function of the dimuon invariant mass square q^2 by BABAR [8], Belle [9] and CDF [10], and the current situation is specially exemplified in Fig. 4. As shown in Fig. 4, the fitted $d\mathcal{A}'_{FB}(B \rightarrow K^*\mu^+\mu^-)/d\hat{s}$ from Belle is generally higher than the SM expectation in whole q^2 bins, while the CDF fitted result is consistent with the SM prediction in some q^2 bins and it is higher than the SM prediction in some other q^2 bins. Especially, in the region of $0 \leq \hat{s} \leq 0.072$ (i.e. $0 \text{ GeV}^2 \leq q^2 \leq 2 \text{ GeV}^2$), the CDF and Belle measurements favor a positive value, whereas the sign of the SM prediction for $d\mathcal{A}'_{FB}(B \rightarrow K^*\mu^+\mu^-)/d\hat{s}$ is negative. It is interesting to find that the RPV coupling $\lambda'_{2i3}\lambda_{2i2}^*$ could accommodate positive $d\mathcal{A}_{FB}(B \rightarrow K^*\mu^+\mu^-)/d\hat{s}$ in the region of $0 \leq \hat{s} \leq 0.072$.

As for the s-channel sneutrino exchange couplings $\lambda_{i22}\lambda_{i23}^*$ and $\lambda_{i22}^*\lambda_{i32}$, the constraints from

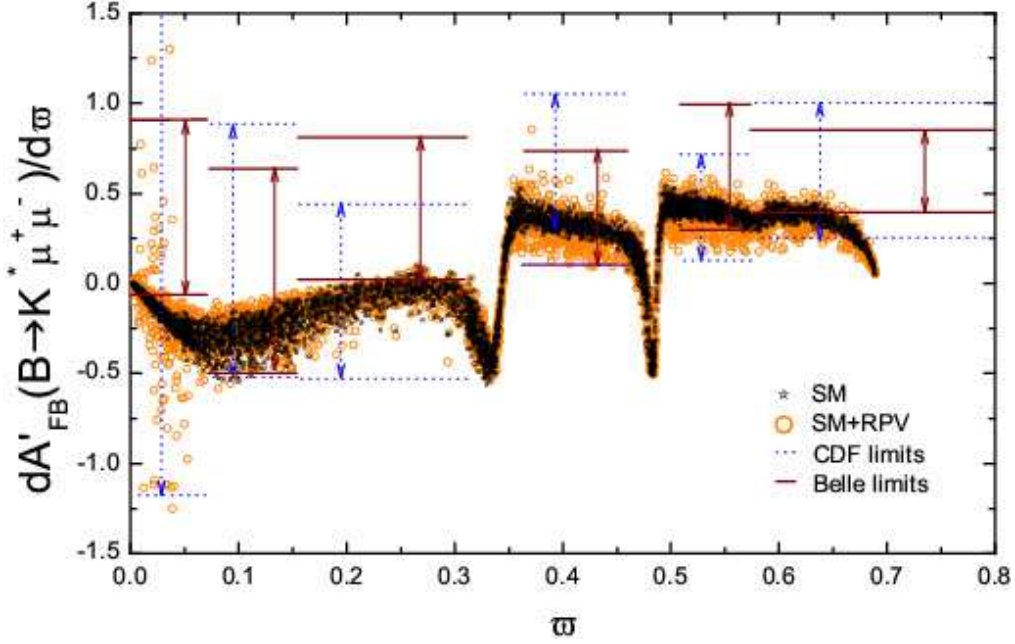


Figure 4: $\mathcal{A}_{FB}(B \rightarrow K^* \mu^+ \mu^-)$ including RPV coupling $\lambda'_{2i2} \lambda'^*_{2i3}$ versus the 90% CL data: CDF(cyan) and Belle(purple).

$\mathcal{B}(B \rightarrow \mu^+ \mu^-)$ are rather restrictive. In Ref. [23], we obtained that both the couplings have negligible contribution to $\mathcal{B}(B \rightarrow K^* \mu^+ \mu^-)$, and only have distinguishable effects on $d\mathcal{B}(B \rightarrow K \mu^+ \mu^-)/d\hat{s}$ at the high \hat{s} region. However, these coupling effects are further constrained by considering the 90% CL new experimental bound of $\mathcal{B}(B_s \rightarrow \mu^+ \mu^-)$ and their effects in $\mathcal{B}(B \rightarrow K^{(*)} \mu^+ \mu^-)$ decays are compatible with hadronic uncertainties. The $\lambda_{i22} \lambda'^*_{i23}$ coupling effects on $d\mathcal{B}(B \rightarrow K \mu^+ \mu^-)/d\hat{s}$ are displayed in Fig. 5, and we see that $\lambda_{i22} \lambda'^*_{i23}$ coupling effects are difficult to distinguish from the SM prediction in the high \hat{s} region. $\lambda'^*_{i22} \lambda'_{i32}$ coupling effects on $d\mathcal{B}(B \rightarrow K \mu^+ \mu^-)/d\hat{s}$ are similar to $\lambda_{i22} \lambda'^*_{i23}$ effects, thus we will not show them again.

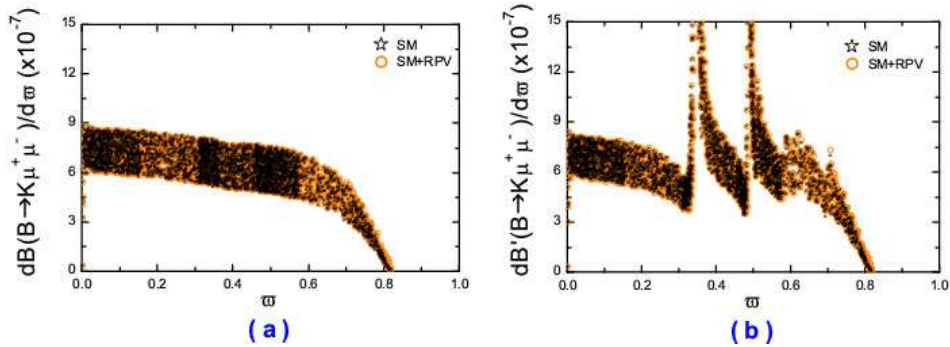


Figure 5: The effects of RPV coupling $\lambda_{i22} \lambda'^*_{i23}$ due to the squark exchange in $B \rightarrow K \mu^+ \mu^-$.

3.2 RPC MI effects

Now we study RPC MI effects in $B_s \rightarrow \mu^+ \mu^-$ and $B \rightarrow K^{(*)} \mu^+ \mu^-$ decays in the MSSM with large $\tan\beta$. The eight kinds of MIs $(\delta_{AB}^{u,d})_{23}$ with $(A, B) = (L, R)$ contribute to $B \rightarrow K^{(*)} \mu^+ \mu^-$ decays, but only three kinds of MIs $(\delta_{LL}^u)_{23}$, $(\delta_{LL}^d)_{23}$ and $(\delta_{RR}^d)_{23}$ contribute to $B_s \rightarrow \mu^+ \mu^-$ decay. We will only consider the contributions of $(\delta_{LL}^u)_{23}$, $(\delta_{LL}^d)_{23}$ and $(\delta_{RR}^d)_{23}$ MIs to $B_s \rightarrow \mu^+ \mu^-$ and $B \rightarrow K^{(*)} \mu^+ \mu^-$ decays in this work. The experimental data shown in Eq. (18) will be used to constrain the three kinds of MI parameters.

MI coupling $(\delta_{LL}^u)_{23}$ has negligible effects on $\mathcal{B}(B_s \rightarrow \mu^+ \mu^-)$ and $\mathcal{B}(B \rightarrow K \mu^+ \mu^-)$, but it could have large effects in the $B \rightarrow K^* \mu^+ \mu^-$ decay. Therefore the bounds of $(\delta_{LL}^u)_{23}$ are entirely obtained from $\mathcal{B}(B \rightarrow K^* \mu^+ \mu^-)$. However, for $(\delta_{LL}^d)_{23}$ and $(\delta_{RR}^d)_{23}$ MI parameters, the constraints by $\mathcal{B}(B \rightarrow K^{(*)} \mu^+ \mu^-)$ are rather weak, which are mainly derived from $\mathcal{B}(B_s \rightarrow \mu^+ \mu^-)$. The constrained spaces of $(\delta_{LL}^u)_{23}$, $(\delta_{LL}^d)_{23}$ and $(\delta_{RR}^d)_{23}$ are displayed in Fig. 6. As shown in Fig. 6, both phases and moduli of three MIs are obviously constrained by the branching ratios given in Eq. (18), and the bounds on the three moduli are $|(\delta_{LL}^u)_{23}| \leq 0.14$, $|(\delta_{LL}^d)_{23}| \leq 0.73$ and $|(\delta_{RR}^d)_{23}| \leq 0.78$. Noted that the very strong constraints on the phases of $(\delta_{LL,RR}^d)_{23}$ MIs arise from ΔM_s , $\Delta \Gamma_s$ and $\phi_s^{J/\psi\phi}$ [30], which are about $\phi_{LL,RR}^d \in [20^\circ, 80^\circ] \cup [-160^\circ, -100^\circ]$. If considering the strong constrained phases from ΔM_s , $\Delta \Gamma_s$ and $\phi_s^{J/\psi\phi}$, we have $|(\delta_{LL}^d)_{23}| \leq 0.73$ and $|(\delta_{RR}^d)_{23}| \leq 0.70$. The upper limits of $|(\delta_{LL,RR}^d)_{23}|$ are consistent with the ones from ΔM_s , $\Delta \Gamma_s$ and $\phi_s^{J/\psi\phi}$ [30], nevertheless the lower limits of $|(\delta_{LL,RR}^d)_{23}|$ are not constrained by the upper limit of $\mathcal{B}(B_s \rightarrow \mu^+ \mu^-)$ at the 90% CL.

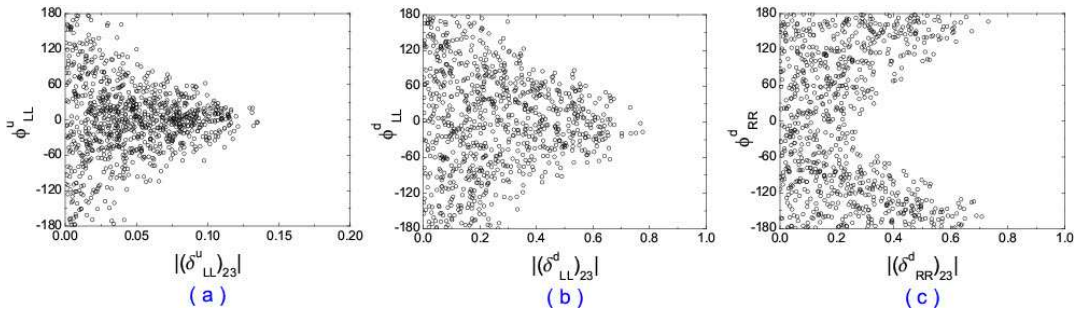


Figure 6: The allowed parameter spaces of $(\delta_{LL}^u)_{23}$, $(\delta_{LL}^d)_{23}$ and $(\delta_{RR}^d)_{23}$ MI parameters constrained by $\mathcal{B}(B_s \rightarrow \mu^+ \mu^-)$ and $\mathcal{B}(B \rightarrow K^{(*)} \mu^+ \mu^-)$ at the 90% CL, and the RPC phase is given in degree.

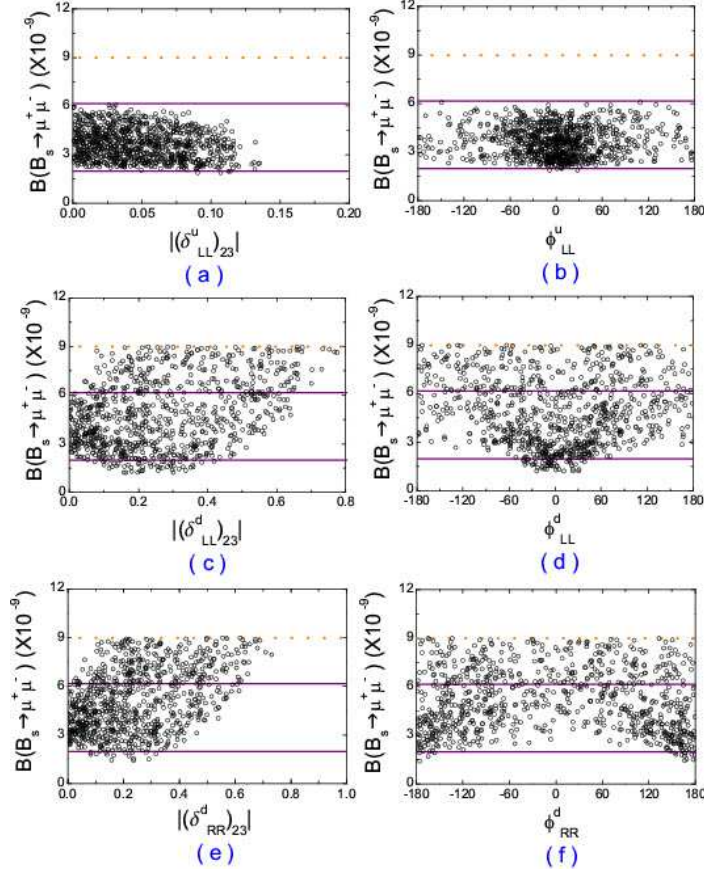


Figure 7: The constrained MI effects on $\mathcal{B}(B_s \rightarrow \mu^+\mu^-)$. The orange(violet) horizontal dashed(solid) lines denote the limits of the measurements(SM predictions) at the 90% CL.

Now we analysis the $(\delta_{LL}^u)_{23}$, $(\delta_{LL}^d)_{23}$ and $(\delta_{RR}^d)_{23}$ MI effects on $\mathcal{B}(B_s \rightarrow \mu^+\mu^-)$. The sensitivities of $\mathcal{B}(B_s \rightarrow \mu^+\mu^-)$ to both moduli and phases of three MIs are displayed in Fig. 7. From Figs. 7 (a-b), we can see that $(\delta_{LL}^u)_{23}$ MI has negligible effects on $\mathcal{B}(B_s \rightarrow \mu^+\mu^-)$, and $\mathcal{B}(B_s \rightarrow \mu^+\mu^-)$ is not sensitive to both modulus and phase of $(\delta_{LL}^u)_{23}$. If the 68% CL experimental determination $\mathcal{B}(B_s \rightarrow \mu^+\mu^-) = (1.8_{-0.9}^{+1.1}) \times 10^{-8}$ [1] by CDF collaboration were taken, the allowed parameter space of $(\delta_{LL}^u)_{23}$ would be excluded. As shown in Figs. 7 (c-f), $(\delta_{LL,RR}^d)_{23}$ couplings are constrained by the upper limit of $\mathcal{B}(B_s \rightarrow \mu^+\mu^-)$, and $\mathcal{B}(B_s \rightarrow \mu^+\mu^-)$ has moderate sensitivities to both the moduli and phases of $(\delta_{LL,RR}^d)_{23}$. The minimum value of $\mathcal{B}(B_s \rightarrow \mu^+\mu^-)$ may present when $|(\delta_{LL}^d)_{23}| \in [0.1, 0.4]$ and $|\phi_{LL}^d| \leq 45^\circ$ or $|(\delta_{RR}^d)_{23}| \in [0.07, 0.33]$ and $|\phi_{RR}^d| \geq 150^\circ$.

Then we analyze the constrained $(\delta_{LL}^u)_{23}$, $(\delta_{LL}^d)_{23}$ and $(\delta_{RR}^d)_{23}$ MI effects in the $B \rightarrow K^{(*)}\mu^+\mu^-$ decays. Using the constrained parameter spaces shown in Fig. 6, we will give the

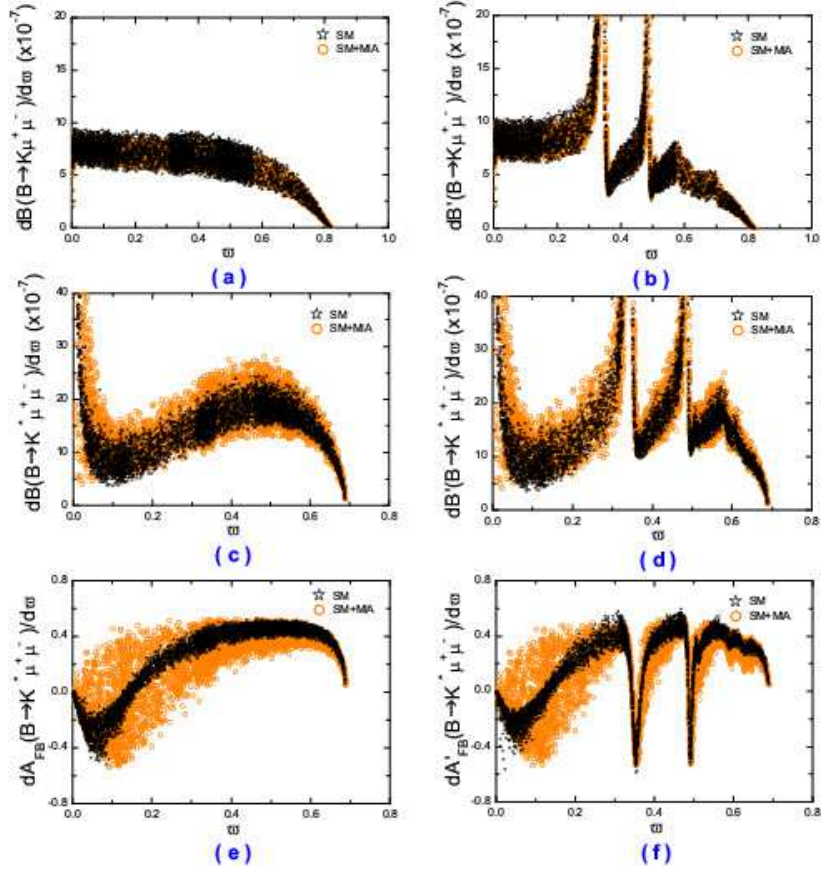


Figure 8: The constrained $(\delta_{LL}^u)_{23}$ MI effects in $B \rightarrow K^{(*)}\mu^+\mu^-$ decays, and ϖ denotes \hat{s} .

MSSM predictions to the dimuon invariant mass spectra of the decay width and the dimuon forward-backward asymmetries of $B \rightarrow K^{(*)}\mu^+\mu^-$ decays in the MI approximation. $(\delta_{LL}^u)_{23}$ MI contributions to $B \rightarrow K^{(*)}\mu^+\mu^-$ are presented in Figs. 8, and we can see that the contribution of the constrained $(\delta_{LL}^u)_{23}$ MI to $d\mathcal{B}(B \rightarrow K\mu^+\mu^-)/d\hat{s}$ is compatible with the theoretical uncertainties and thus is indistinguishable. On the other hand, its contribution to $d\mathcal{B}(B \rightarrow K^*\mu^+\mu^-)/d\hat{s}$ and $d\mathcal{A}_{FB}(B \rightarrow K^*\mu^+\mu^-)/d\hat{s}$ could be significant, as shown in Figs. 8 (c-f), when theoretical uncertainties are considered. It is of interest to note that the contribution to $d\mathcal{A}_{FB}(B \rightarrow K^*\mu^+\mu^-)/d\hat{s}$ at the low \hat{s} is favored by the current experimental measurements [9, 10].

Since $(\delta_{LL}^d)_{23}$ and $(\delta_{RR}^d)_{23}$ MIs have similar effects in $B \rightarrow K^{(*)}\mu^+\mu^-$, we only show the $(\delta_{LL}^d)_{23}$ MI effects in Fig. 9 for instance. From Figs. 9 (a-b), we can see that $d\mathcal{B}(B \rightarrow K\mu^+\mu^-)/d\hat{s}$ could be slightly suppressed in all \hat{s} region by the $(\delta_{LL}^d)_{23}$ MI coupling. As shown in Figs. 9 (c-d), $d\mathcal{B}(B \rightarrow K^*\mu^+\mu^-)/d\hat{s}$ could be increased much in the low \hat{s} region, but slightly

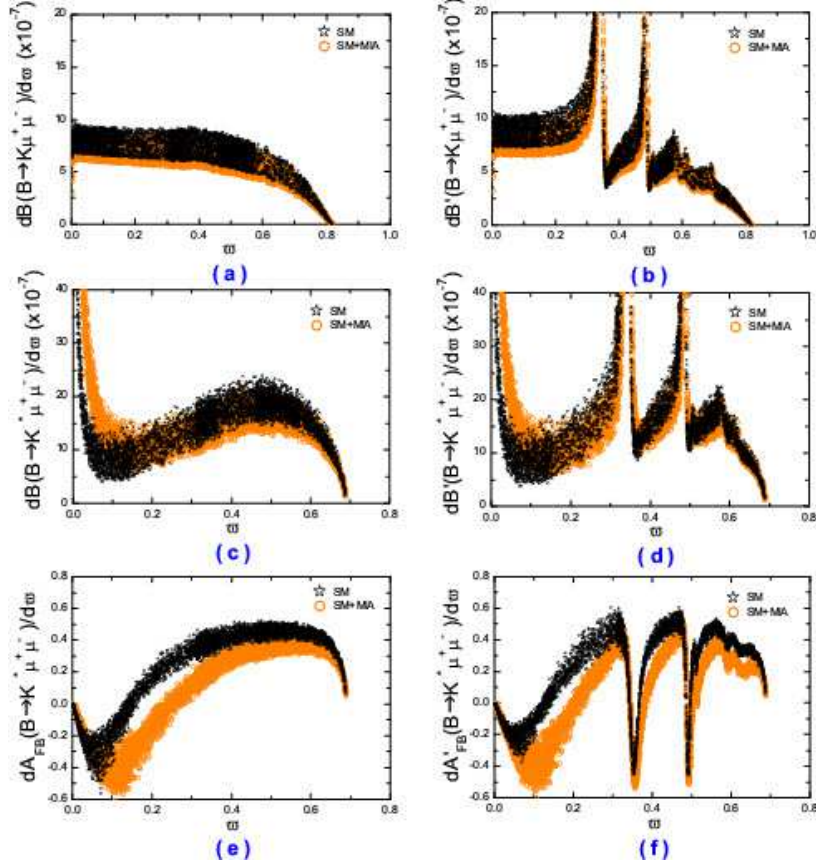


Figure 9: The constrained $(\delta_{LL}^d)_{23}$ MI effects in $B \rightarrow K^{(*)}\mu^+\mu^-$ decays, and ϖ denotes \hat{s} .

decreased in the high \hat{s} region by the $(\delta_{LL}^d)_{23}$ MI. Figs. 9 (e-f) show us that the constrained $(\delta_{LL}^d)_{23}$ MI has significant effects on $d\mathcal{A}_{FB}(B \rightarrow K^*\mu^+\mu^-)/d\hat{s}$ when $\hat{s} > 0.07$, which could be distinctly lower than the SM prediction. However, such effects due to $(\delta_{LL}^d)_{23}$ MI is not favored by the the current experimental measurements [9, 10].

4 Conclusions

Motivated by the recent searches of $\mathcal{B}(B_s \rightarrow \mu^+\mu^-)$ by the CDF, LHCb and CMS collaborations, we have studied $B_s \rightarrow \mu^+\mu^-$ and $B \rightarrow K^{(*)}\mu^+\mu^-$ decays in the MSSM with and without R-parity. In the MSSM without R-parity, we have found that the relevant RPV coupling bounds are improved by the present new measurements. The further constrained RPV coupling due to t-channel squark exchange still has significant effects in $B \rightarrow K^{(*)}\mu^+\mu^-$ decays, and the Belle measurement of $d\mathcal{A}_{FB}(B \rightarrow K^*\mu^+\mu^-)/d\hat{s}$ in the region of $0 \text{ GeV}^2 \leq q^2 \leq 2 \text{ GeV}^2$ could

be accommodated by the squark exchange coupling. The further constrained couplings due to s-channel sneutrino exchange could have large effects in $B_s \rightarrow \mu^+ \mu^-$, but have negligible effects in $B \rightarrow K^{(*)} \mu^+ \mu^-$ decays.

In the MSSM with R-parity, three MI parameters $(\delta_{LL}^u)_{23}$, $(\delta_{LL}^d)_{23}$ and $(\delta_{RR}^d)_{23}$ suffer the combined constraints from the present data of $\mathcal{B}(B_s \rightarrow \mu^+ \mu^-)$ and $\mathcal{B}(B \rightarrow K^{(*)} \mu^+ \mu^-)$. The constrained $(\delta_{LL}^u)_{23}$ MI could give large $d\mathcal{A}_{FB}(B \rightarrow K^* \mu^+ \mu^-)/d\hat{s}$ in the low \hat{s} region in favor of the experimental measurements from Belle collaboration. $d\mathcal{B}(B \rightarrow K^* \mu^+ \mu^-)/d\hat{s}$ could be significantly increased in the low \hat{s} region but suppressed in the high \hat{s} region by the constrained $(\delta_{LL,RR}^d)_{23}$ MIs. The constrained $(\delta_{LL,RR}^d)_{23}$ MIs still have very large effects on $d\mathcal{A}_{FB}(B \rightarrow K^* \mu^+ \mu^-)/d\hat{s}$, which could be distinctly decreased in almost all \hat{s} region, and this is disfavored by the current experimental measurements.

In the immediate future, the LHC is expected to become sensitive to $\mathcal{B}(B_s \rightarrow \mu^+ \mu^-)$. Accurately measurements of the $B_s \rightarrow \mu^+ \mu^-$ and $B \rightarrow K^{(*)} \mu^+ \mu^-$ decays could further shrink or reveal the parameter spaces of MSSM with and without R-parity.

Acknowledgments

The work is supported by National Science Foundation (Nos. 11105115, 11147136 and 11075059) and Project of Basic and Advanced, Technology Research of Henan Province (No. 112300410021).

Appendix: Input parameters

The input parameters are summarized in Table 2. For the RPC MI effects, we choose the five free parameters $m_0 = 300 \text{ GeV}$, $m_{1/2} = 200 \text{ GeV}$, $A_0 = 0$, $\text{sign}(\mu) > 0$ and $\tan\beta = 50$. All other MSSM parameters are then determined according to the constrained MSSM scenario as implemented in the program package SUSPECT [34]. For the form factors involving the $B \rightarrow K^{(*)}$ transitions, we will use the recently light-cone QCD sum rules (LCSRs) results [31, 32], which are renewed with radiative corrections to the leading twist wave functions and SU(3) breaking effects. For the q^2 dependence of the form factors, they can be parameterized in terms of simple formulae with two or three parameters. The expression can be found in Ref. [31, 32]. In our numerical data analysis, the uncertainties induced by $F(0)$ are also considered.

Table 2: Default values of the input parameters.

$m_{B_s} = 5.370 \text{ GeV}, \quad m_{B_d} = 5.279 \text{ GeV}, \quad m_{B_u} = 5.279 \text{ GeV}, \quad m_W = 80.425 \text{ GeV},$	
$m_{K^\pm} = 0.494 \text{ GeV}, \quad m_{K^0} = 0.498 \text{ GeV}, \quad m_{K^{*\pm}} = 0.892 \text{ GeV}, \quad m_{K^{*0}} = 0.896 \text{ GeV},$	
$\overline{m}_b(\overline{m}_b) = (4.19_{-0.06}^{+0.18}) \text{ GeV}, \quad \overline{m}_s(2\text{GeV}) = (0.100_{-0.020}^{+0.030}) \text{ GeV},$	
$\overline{m}_u(2\text{GeV}) = 0.0017 \sim 0.0031 \text{ GeV}, \quad \overline{m}_d(2\text{GeV}) = 0.0041 \sim 0.0057 \text{ GeV},$	
$m_e = 0.511 \times 10^{-3} \text{ GeV}, \quad m_\mu = 0.106 \text{ GeV}, \quad m_{t,pole} = 172.9 \pm 1.1 \text{ GeV}.$	[26]
$\tau_{B_s} = (1.466 \pm 0.059) \text{ ps}, \quad \tau_{B_d} = (1.530 \pm 0.009) \text{ ps}, \quad \tau_{B_u} = (1.638 \pm 0.011) \text{ ps}.$	[26]
$ V_{tb} \approx 0.99910, \quad V_{ts} = 0.04161_{-0.00078}^{+0.00012}.$	[26]
$\sin^2\theta_W = 0.22306, \quad \alpha_e = 1/137.$	[26]
$f_{B_s} = 0.230 \pm 0.030 \text{ GeV}.$	[33]

References

- [1] T. Aaltonen *et al.* (CDF collaboration), Phys. Rev. Lett. **107**, 191801 (2011).
- [2] S. Chatrchyan *et al.* (CMS collaboration), arXiv:1107.5834.
- [3] R. Aaij *et al.* (LHCb collaboration), arXiv:1112.0511.
- [4] R. Aaij *et al.* (LHCb collaboration), Phys. Lett. **B699** 330 (2011).
- [5] CMS and LHCb collaborations, CMS-PAS-BPH-11-019, LHCb-CONF-2011-047, CERN-LHCb-CONF-2011-047.
- [6] V. Abazov *et al.* (DØ collaboration), Phys. Lett. **B693**, 539 (2010); T. Aaltonen *et al.* (CDF collaboration), Phys. Rev. Lett. **100**, 101802 (2008).
- [7] A. J. Buras, M. V. Carlucci, S. Gori and G. Isidori, JHEP **1010**, 009 (2010).
- [8] B. Aubert *et al.* (BABAR collaboration), Phys. Rev. **D79**, 031102 (2009).
- [9] J. T. Wei *et al.* (Belle collaboration), Phys. Rev. Lett. **103**, 171801 (2009).
- [10] T. Aaltonen *et al.* (CDF collaboration), Phys. Rev. Lett. **106**, 161801 (2011).

- [11] G. Burdman, Phys. Rev. **D57**, 4254 (1998).
- [12] M. Beneke, T. Feldmann and D. Seidel, Nucl. Phys. **B612**, 25 (2001).
- [13] A. Ali, P. Ball, L. T. Handoko and G. Hiller, Phys. Rev. **D61**, 074024 (2000).
- [14] D. Palle, arXiv:1111.1639.
- [15] C. Beskidt *et al.*, Phys. Lett. **B705**, 493 (2011).
- [16] A. G. Akeroyd, F. Mahmoudi and D. M. Santos, arXiv:1108.3018.
- [17] W. Altmannshofer, M. Carena, S. Gori and A. de la Puente, arXiv:1107.3814.
- [18] A. K. Alok *et al.*, JHEP **1111**, 121 (2011).
- [19] E. Lunghi and A. Soni, JHEP **1011**, 121 (2010).
- [20] Q. Chang, X. Q. Li and Y. D. Yang, JHEP **1004**, 052 (2010).
- [21] W. Altmannshofer *et al.*, Nucl. Phys. **B830**, 17-94 (2010).
- [22] W. Altmannshofer *et al.*, JHEP **0901**, 019 (2009).
- [23] Y. G. Xu, R. M. Wang and Y. D. Yang, Phys. Rev. **D74**, 114019 (2006).
- [24] F. Gabbiani, E. Gabrielli, A. Masiero and L. Silvestrini, Nucl. Phys. **B477**, 321 (1996).
- [25] F. Gabbiani and A. Masiero, Nucl. Phys. **B322**, 235 (1989).
- [26] K. Nakamura *et al.* (Particle Data Group), J. Phys. **G37**, 075021 (2010) and 2011 partial update for the 2012 edition.
- [27] C. Bobeth, T. Ewerth, F. Kruger and J. Urban, Phys. Rev. **D64**, 074014 (2001).
- [28] E. Lunghi, A. Masiero, I. Scimemi and L. Silvestrini, Nucl. Phys. **B568**, 120-144 (2000).
- [29] P. L. Cho, M. Misiak and D. Wyler, Phys. Rev. **D54**, 3329-3344 (1996).
- [30] R. M. Wang, Y. G. Xu, Q. Chang and Y. D. Yang, Phys. Rev. **D83**, 095010 (2011).
- [31] P. Ball and R. Zwicky, Phys. Rev. **D71**, 014015 (2005).

- [32] P. Ball and R. Zwicky, Phys. Rev. **D71**, 014029 (2005).
- [33] S. Hashimoto, Int. J. Mod. Phys. **A20**, 5133-5144 (2005).
- [34] A. Djouadi, J. L. Kneur and G. Moultaka, Comput. Phys. Commun. **176**, 426 (2007).